Voltage Instability – the Different Shapes of the "Nose"

Sandro Corsi
CESI – Italy

Glauco N. Taranto
COPPE/UFRJ – Brazil

***Abstract*--This paper was elaborated to enlarge the understanding on the dependence of the shape of the "nose" of a Power-Voltage (PV) curve in a given EHV bus, by the power system dynamics. The paper shows that the local control loops are strongly involved in the voltage instability phenomenon and how they modify the shape of the nose curve. The paper also analyzes how these local control loops, together with the local load characteristics, impact on the "speed to run" the PV curves and on the stability of their equilibrium points. A detailed analysis of the nose shapes and characteristics is preliminarily performed for each relevant control loop and different types of loads. The subsequent analyses refer to a realistic load representation and compare, in terms of nose characteristics, the results of some Italian EHV buses with a proposed equivalent dynamic model, giving evidence of the strong correlation between the two and confirming the relevant differences with the corresponding static nose curves. The focus given in the paper was mainly motivated by the new opportunities to estimate the proximity to voltage instability from fast and synchronized bus measurements, provided by a local Phasor Measurement Unit (PMU).**

***Index Terms* — Voltage Stability, Dynamic Simulation, Long-term analysis, PMU, OEL, OLTC.**

I. Introduction

THE subject of voltage instability in electrical transmission networks has been extensively and comprehensively treated in some books [1–3] and in many papers for at least the last two decades. A fairly complete list of publications on the subject up to 1996 can be found in [4]. In the past, much effort was put for the correct description of the phenomenon that, in the first works, had its interpretation prevailed from static mathematical models. Subsequently, fruitful discussions were opened between supporters of the adequacy of static models and supporters of dynamic models to better represent the phenomenon. Today, there is a consensus that exclusive static models deprived of closed loop controls are insufficient to fully describe the voltage instability as it develops on a real electric network.

We fill that the literature still lacks a wider and detailed analysis referring to the dynamic aspects that greatly contribute and impact on the voltage instability process and be able to give evidence of their specific contribution to the phenomenon. Some relevant publications [5-9] deals with this problem and show the relevance of a dynamic analysis through examples that cover specific aspects linked to the voltage instability mechanisms. Nevertheless, those examples are far from a complete and organic overview of each control loop having a relevant impact on the phenomenon in practice.

Recently the voltage stability subject has returned with much interest from a new perspective given by the commercially available, cost-reduced technology of Phasor Measurement Units (PMU) [10], for the fast computation of real-time voltage instability risk indicators. The possibility to quickly compute, at a given EHV bus, the corresponding voltage instability proximity indicators, based on local phasor measurements of voltage and current is of great interest for control and protection of the electrical network. This subject has been investigated in [11-14], and the various recent studies refer to a simple network model composed by a load bus and the Thevenin equivalent seen from this bus, as depicted in Fig.1. This is the conventional system equivalent structure to which a large variety of books and papers refer, when introducing the basics on voltage stability.

Based on this simple equivalent the proposed analyses consider the well-known PV curve (commonly known from its nasal form) obtained by increasing the load, and considering, under certain circumstances, the maximum loadability point as the limit of voltage stability [12,14]. These works present their methodology referring to the classic static PV curve for the load buses, that can be approximately described by a fourth-order algebraic equation, whose all the points are stable equilibria and the generator voltage is held constant. Therefore, the dynamical aspects linked to the voltage instability phenomenon seem frequently overlooked in the choice of the models to study the problem.

On the contrary, we consider relevant, independently of the adopted method to define the voltage instability indicator, to base the analysis on a credible equivalent network model that shows loadability conditions often significantly different from those indicated by the static model. In fact the "nose" assumes diverse forms according to the dynamic aspects and the load characteristics adopted. Moreover, for a given load increase, there is a variety of "noses" consisting, even in some small portions, of unstable points, and ran by diverse speeds driven by different closed-loop control configurations. Therefore, the analysis framework is very interesting and complex.

This paper presents a comprehensive analysis for possible equivalent models seen from a bus, as representative as possible of the actual systems, highlighting how the dynamic aspects of the generator Over Excitation Limits (OEL) and of

G. N. Taranto acknowledges the financial support provided by CNPq and CESI during his sabbatical leave of absence.

S. Corsi is with CESI Spa., Milan, Italy (corsi@cesi.it).

G. N. Taranto is with Federal University of Rio de Janeiro, COPPE/UFRJ, 21945-970, Rio de Janeiro, RJ, Brazil (tarang@coep.ufrj.br).

the On Load Tap Changers (OLTC) transformers [8,9] impact on the PV curves, in particular to the parts of more interest for the phenomenon of voltage instability. It also highlights the impact on the "nose" shape, on the "speed to run" the noses, and on the stability of individual points of the curve, by the control dynamics combined with the characteristic of the loads.

Much of the information hereafter presented is presumably known, however, we reinstate that one organic framework on the factors that impact on the shape and characteristic of the PV curves, to be an important and useful contribution to the subject. In synthesis, we want objectively to give evidence, not only referring to the simple system based on the Thevenin equivalent, but also to the high-voltage Italian electrical system dynamically modeled, to the results qualitatively depicted in Fig.2.

More specifically the objective of the paper is to give evidence and confirmation to the following statements:

a) The generic static PV curve of a load bus, based on the assumption that the equivalent (Fig.1) Thevenin generator "seen" from the bus being ideal and having dynamics neglected, describes operating points often not coherent to the actual physical system. Referring to the common way to represent real loads, the static PV curve at an EHV bus indicates the maximum loadability point with values of active power higher with respect to physical possibilities. Furthermore, the points of the static PV curves are stable equilibria, fact that does not occur in a more representative dynamic model.

b) Considering the same equivalent model of item a) but with a non-ideal generator under an AVR control with excitation ceiling limit and with a governor under speed regulation: the dynamic PV curve of the load bus approaches the static curve referred in item a) as much higher is the AVR gain, and till when the ceiling limit is not reached. After excitation saturation, the PV curve lies inside the static nose curve. According to the characteristic of the load, some points on the PV curve can be unstable equilibria (Fig.2, part of the curves on the left of the "X" mark), with or without the ceiling saturation.

c) Considering the model of item b) but with a realistic AVR with OEL: increasing the load, the OEL significantly modify the PV nose shape, lowering the maximum loadability and contributing to the instability of the low voltage PV curve equilibrium points. This happens for most of the loads (Fig.2, dot-dashed line).

d) At last, we cannot forget the OLTC transformers and their important dynamic model on the determination of the "nose" shape of the PV curve and on the speed to go from one point in the curve to the next, particularly when the OLTC, in the local load bus, works in the vicinity of the maximum power transfer limit (Fig.2, solid line).

The "X" mark in Fig.2 represents the point from which the PV curve points are unstable, and the symbol "V" indicates the speed, at a specific voltage level, the equilibrium point moves according to the load increase. Normally these speed values are such V1 > V2 > V3.

The paper has also the objective to show the coherent results between PV curves obtained from the proposed dynamic equivalent model of the grid seen by a given EHV bus, and from a detailed model representing a very large grid, including the detailed dynamics of various OELs and OLTCs.

The performed analysis is fully oriented to recognize, for each given network structure, the voltage stability margin ("seen" from a given bus) with respect to the operating point. Therefore, the load ramp increase is the way to clearly put in evidence the real limit, instead of severe system contingencies, with transients dominated by a large variety of phenomena, including the voltage degradation/instability. Clearly, the steady state condition after a contingency is a new starting point to be checked against voltage instability by repeating the slow load increase. According to this view, the most significant approach to find the voltage stability limit is to define the system structures and load characteristics to be analyzed by load ramp increase.

The paper presents in appendix the complete static and dynamic data set, and the block diagrams of the voltage and speed regulators of the proposed system equivalent model, such that the readers may be able to reproduce the results, particularly to reconstruct the various shapes of the "noses" presented.

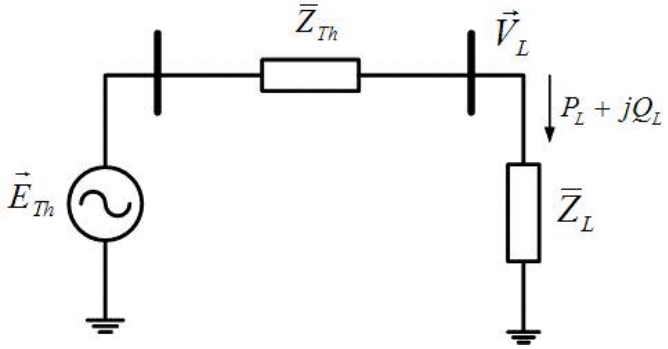

Fig. 1. Two-bus Thevenin Equivalent Circuit

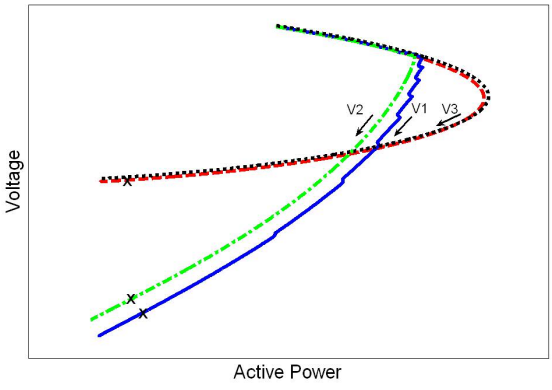

Fig. 2. "Nose" Curves – one obtained from static models (dotted), and the other three obtained from dynamic models. With AVR only (dashed), AVR+OEL (dash-dotted), and AVR+OEL+OLTC (solid).

II. PV Curve Basics

If, for simplicity, the Thevenin impedance in Fig.1 is replaced by a pure reactance X_{Th}, and the Thevenin voltage is assumed constant, it can be shown [9] that the voltage at the load bus varies with respect to the load active power P_L and load reactive power Q_L according to (1).

$$V_L = \sqrt{\frac{E_{Th}^{\ 2}}{2} - Q_L X_{Th} \pm \sqrt{\frac{E_{Th}^{\ 4}}{4} - X_{Th}^{\ 2} P_L^{\ 2} - X_{Th} E_{Th} Q_L}} \qquad (1)$$

For a constant reactive power Fig.3 shows the well know "nose" relating voltage to active power, and Fig.4 shows the nose surface relating voltage to both active and reactive power.

Maximum power transfer to the load occurs at the tip of the nose when the load impedance is equal to the Thevenin impedance in Fig.1, in terms of absolute value.

All the (P, V, Q) points in Fig.4 represent equilibrium points; therefore the instability (solvability) limit is achieved with a load characteristic tangent to the surface. Referring to a P-constant load increase, the tip of the nose represents both the maximum loadability and the voltage instability limit. A pure Z-constant load always intersects the "nose parabola", therefore all the points in the curve are stable, even if at very low voltage values.

This paper critically observe on the use of these static curves to recognize the real system voltage instability limit and proposes an equivalent dynamic model to better fit the real phenomenon.

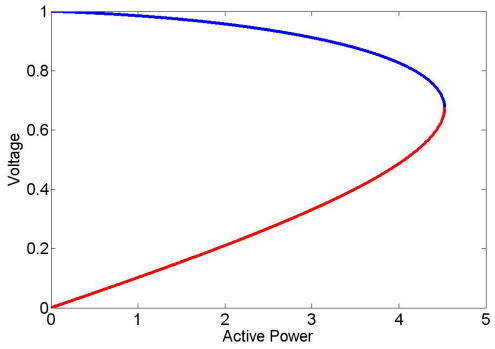

Fig. 3. The well-known Nose Curve

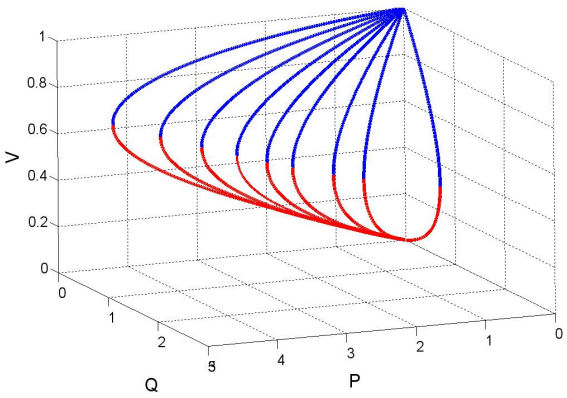

Fig. 4. Three-Dimension Nose Curves

III. The Proposed Equivalent System

This section proposes a one-machine dynamic equivalent model that has two objectives: first to aggregate dynamic aspects to the static equivalent model (as depicted in Fig.1) for the analyses of voltage stability based on Thevenin equivalents, and second, to serve as a test system for the simulations of PV curves.

Fig.5 shows the one-line diagram of the proposed dynamic equivalent system. It consists of a 370MVA/20kV round-rotor synchronous machine (six-order model), one 380MVA-20kV /400kV step-up transformer, one 460MVA-400kV/132kV step-down transformer, six parallel 64MVA-132kV/20kV OLTC distribution transformers, and two parallel 400kV /100km overhead transmission lines. The data for the network and for the dynamic components, as well as the block diagrams of the voltage and speed regulators are given in appendix. The data utilized in the numerical simulations represent actual components taken from the Italian electric system.

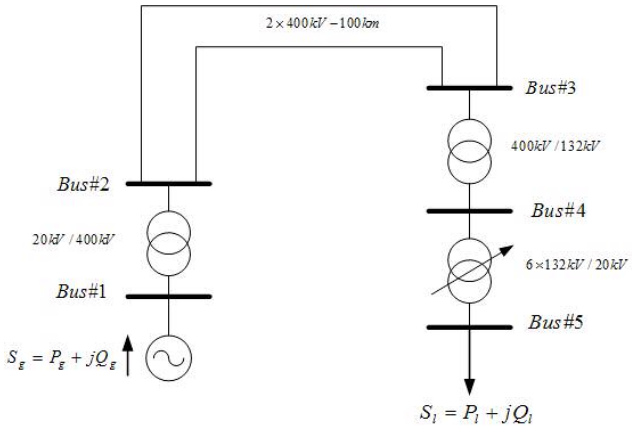

Fig. 5. One-Line Diagram of the Test System

IV. Analysis of PV Curves for the Test System

This section presents a comprehensive analysis of nose curves for the test system shown in Fig.5. The presentation of the results is organized according to the closed-loop controls that are active. Three cases are defined as follows:

- Case 1 – OLTC and OEL in service;
- Case 2 – OLTC out of service and OEL in service;
- Case 3 – OLTC and OEL out of service.

Cases 1 and 2 represent realistic operating conditions of a power system, where the OELs are always in service while the OLTCs may be blocked. The Case 3 is a reference case, since it sufficiently represents the static PV curve (actually the real static curve corresponds to Case 3 with the AVR having an integral control law without ceiling limit).

In all cases the automatic voltage regulator (AVR) and the speed regulator are in service. Moreover, these three cases are compared to each other according to the:

- Load type characteristic;
- Initial operating condition;
- Voltage bus level.

Two initial operating conditions are considered. Condition 1 when the initial load is 160MW (0.43pu) and 0Mvar, and Condition 2 when the initial load is 280MW (0.76pu) and 20Mvar. Also two buses are considered, the EHV bus (Bus#3) and the load bus (Bus#5). Finally, with respect to the load type, the common ZIP model is used. 100% P-constant, 100% I-constant and 100% Z-constant, for both active and reactive power, are considered to analyze their specific effects.

For all the cases studied the load increase rate is equal to ΔP_L=0.5MW/s and ΔQ_L=0.5Mvar/s according to (2).

$$P_L = (P_o + \Delta P_L) \times \left(\frac{V_L}{V_o}\right)^{\alpha} \qquad Q_L = (Q_o + \Delta Q_L) \times \left(\frac{V_L}{V_o}\right)^{\beta} \qquad (2)$$

Where P_o, Q_o and V_o are nominal values, and α and β are constants to model the load type characteristic.

A. Z-Constant Load Type ($\alpha = \beta = 2.0$)

All results in this subsection were obtained with the load represented as Z-constant type. Fig.6 and Fig.7 show the nose curves when the system is in Condition 1 for Bus#3 and Bus#5, respectively. Fig.8 and Fig.9 show the nose curves when the system is in Condition 2 for Bus#3 and Bus#5, respectively.

One can clearly note the large differences in the shape of these curves, particularly at the nose, when the control loops start to operate.

The simulation time for the results presented in Figs.6-9, is 700 seconds. Due to the type of the load the system does not present voltage stability problems. Thus, the nose curves shown in these figures are drawn up to this simulation time.

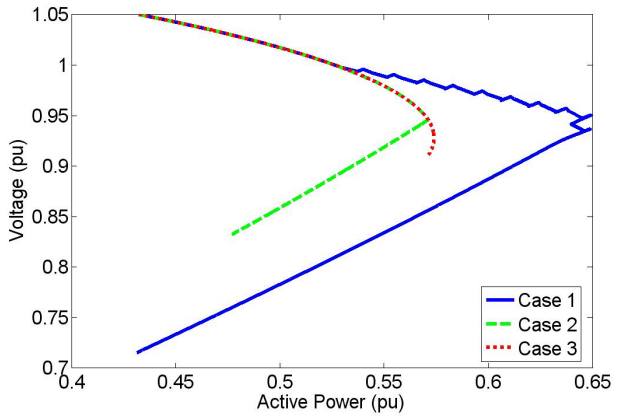

Fig. 6. Nose Curves at Bus#3 for Condition 1 and load as Z-constant

Table I shows the time, in seconds, to reach the maximum power transfer (T_{max}), the time to reach 0.85 pu of voltage in the EHV bus ($T_{0.85}$), the computing collapse (T_{coll}) and the actual time of instability ($T_{s\&g}$). $T_{0.85}$ is particularly important to be recorded because, in general, at this voltage level undervoltage relays normally start to operate. T_{coll} is defined as the time in which the simulation program has numerical difficulties to converge. Often the system crosses the voltage stability limit some time before it. This lead us to define $T_{s\&g}$, which is defined as the maximum time where stopping the load increase and going on with the simulation, the system autonomously evolves to instability. The values shown in Table I are with respect to the nose curves presented in Fig.6.

Table I – Key recorded time (sec) with respect to Fig.6

Case	T_{max}	$T_{0.85}$	T_{coll}	$T_{s\&g}$
1	311	424	∞	∞
2	464	656	∞	∞
3	574	>700	∞	∞

Comments on Fig.6 and Table I

1. The increasing effect of power transfer limit by the OLTC;
2. Voltage deterioration acceleration by the OLTC. Even though the OLTC tries to maintain voltage, it drives the system into operating points where the dynamic mechanisms quickly depress voltage.
3. T_{coll} and $T_{s\&g}$ are infinity because there is no voltage instability problems when loads are represented as Z-constant type.
4. With respect to the curve of Case 2, one can note that the system changes immediately from a situation of increase in power with the increase in the load admittance (or decrease in load impedance, if you will), to a situation of decrease in power with the increase in the load admittance. This is explained by the fact that when the generator reaches its over-excitation limit the equivalent Thevenin impedance, seen from the buses near the load, increases. The synchronous reactance now becomes part (and a big one) of the equivalent Thevenin impedance. At that point the impedance of the load is higher than the equivalent Thevenin impedance and the system is beyond the maximum power transfer limit.
5. The time to reach T_{max} and $T_{0.85}$ is very different among Cases 1, 2 and 3 and the speed to run along the curve of Case 3 is considerably slower with respect to the other two cases.

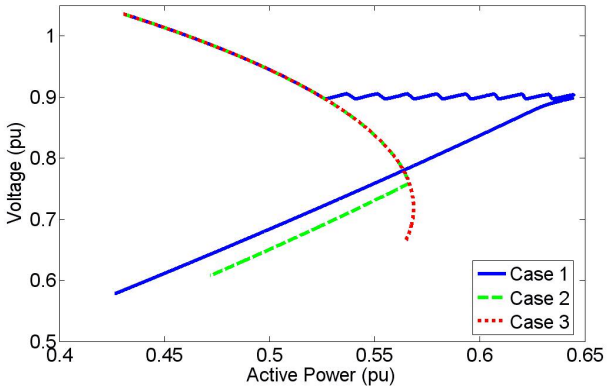

Fig. 7. Nose Curves at Bus#5 for Condition 1 and load as Z-constant

From Fig.7 one can note the actuation of the OLTC in trying to maintain the voltage on Bus#5 at the minimum dead-band value of 0.9 pu. It is clear the effects of this actuation in

the first 8 tap changes. After that, the generator OEL starts to operate and mainly drives the dynamics of the system, thus mitigating the effect of the last 2 tap changes of the OLTC.

Bus#5 shows the relevant difference in terms of voltage lowering with respect to the EHV Bus#3. At Bus#5 the voltage decay is more evident. Moreover, the differences on the nose shapes are markedly evident at Bus#5, as well.

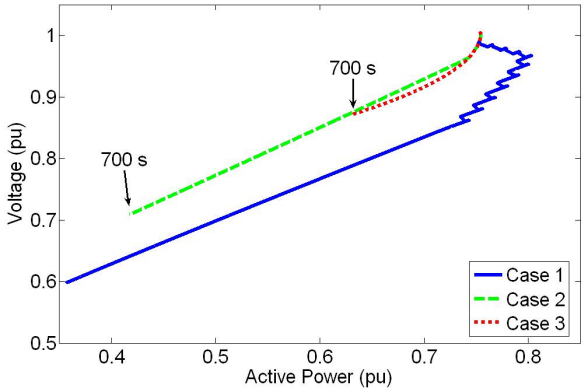

Fig. 8. Nose Curves at Bus#3 for Condition 2 and load as Z-constant

Table II shows the time values for the key points already described. It refers to the nose curves presented in Fig.8.

Table II – Key recorded time (sec) with respect to Fig.8

Case	T_{max}	$T_{0.85}$	T_{coll}	$T_{s\&g}$
1	90	126	∞	∞
2	4	325	∞	∞
3	4	>700	∞	∞

Comments on Fig.8 and Table II

6. Comments 1, 2 and 3 made before are still valid.
7. In this heavier-load initial operating condition the system is very close to the maximum power transfer limit. In this case the OEL actuation (Case 2) occurs when the nose curve is already in its lower part. In this situation the voltage rate of change in Case 2 is higher (e.g., at 700 sec is roughly double) with respect to the one of Case 3.
8. The speed of the voltage lowering is markedly different in all three cases. Case 3 resembles the static PV curve.

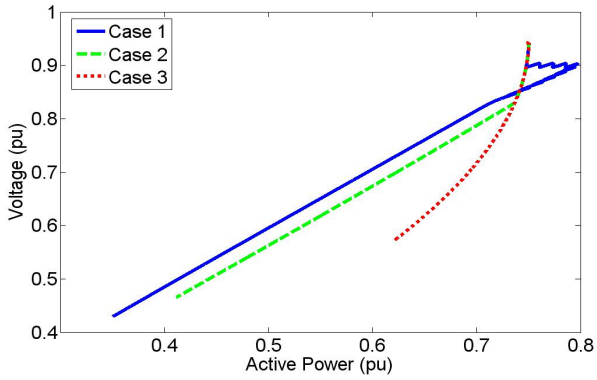

Fig. 9. Nose Curves at Bus#5 for Condition 2 and load as Z-constant

Fig. 9 again puts in evidence the very low voltage value with respect to Fig. 8 related to the EHV Bus.

Fig.10 refers to Case 1 and shows the transients of the OEL, which begins to operate at 89s, and of the OLTC. In the considered working condition, where the OLTC is stepping down and the OEL is starting to limit, occurs a stop on the active power increase at 90s and a fast voltage lowering. The voltage at Bus#3 changes from 0.98pu to 0.85pu in 36s.

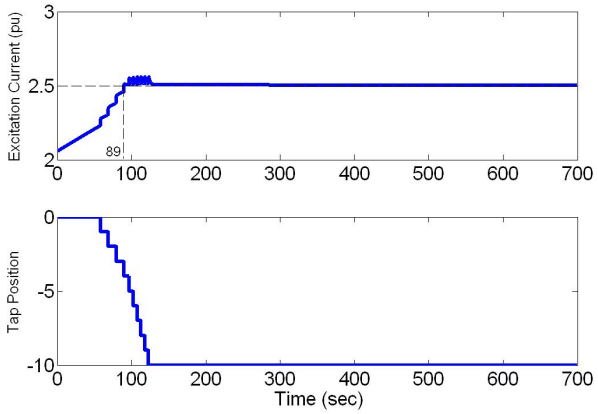

Fig. 10. Excitation Current and Tap Position in Case 1 Simulation

B. *I-constant Load Type ($\alpha = \beta = 1.0$)*

All results in this subsection were obtained with the load represented as I-constant type. Fig.11 and Fig.12 show the nose curves when the system is in Condition 1 for Bus#3 and Bus#5, respectively. Fig.13 and Fig.14 show the nose curves when the system is in Condition 2 for Bus#3 and Bus#5, respectively.

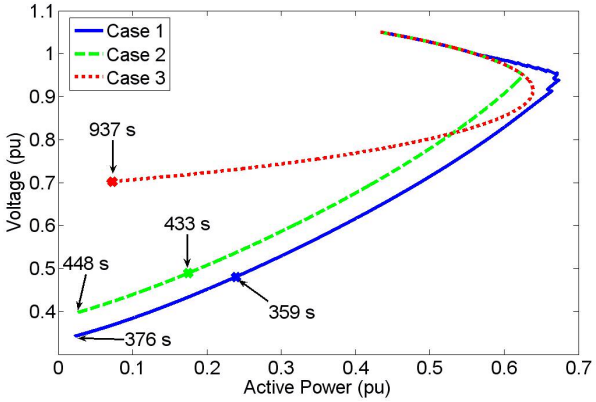

Fig. 11. Nose Curves at Bus#3 for Condition 1 and load as I-constant

Table III shows the times with respect to the simulation results presented in Fig.11.

Table III – Key recorded time (sec) with respect to Fig.11

Case	T_{max}	$T_{0.85}$	T_{coll}	$T_{s\&g}$
1	255	276	376	359
2	292	334	448	433
3	386	553	940	937

Comments on Fig.11 and Table III

9. Comments 1 and 2 are still valid.

10. T_{coll} and $T_{s\&g}$ are finite and different because now the loads are represented as I-constant type and stability problems start to occur, with voltages at very low values.
11. The difference between T_{coll} and $T_{s\&g}$ is about the same for Cases 1 and 2 (17 and 15 seconds, respectively). This difference approaches zero for Case 3 (3 sec).
12. In terms of speed to run along the curves, the Case 3, also representative of the static PV curve, is very slow with respect to Cases 1 and 2, again confirming the distance of the static curve from the real process.

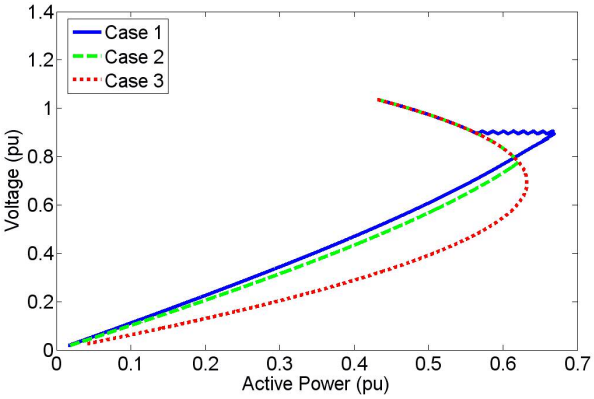

Fig. 12. Nose Curves at Bus#5 for Condition 1 and load as I-constant

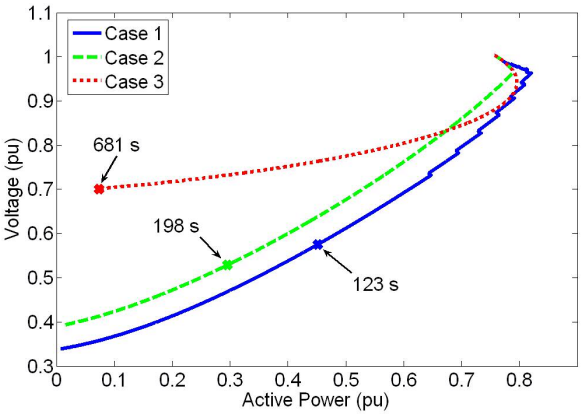

Fig. 13 Nose Curves at Bus#3 for Condition 2 and load as I-constant

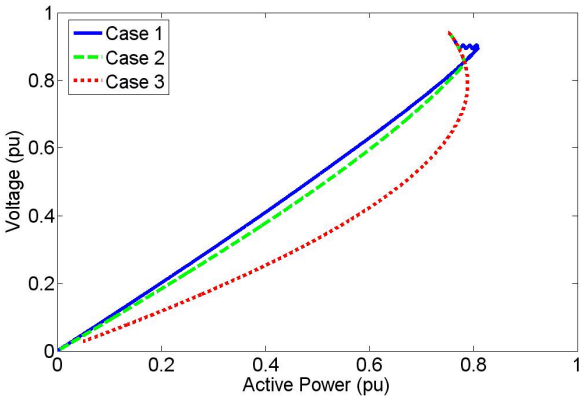

Fig. 14. Nose Curves at Bus#5 for Condition 2 and load as I-constant

Table IV shows the times with respect to the simulation results presented in Fig.13.

Table IV– Key recorded time (sec) with respect to Fig.13

Case	T_{max}	$T_{0.85}$	T_{coll}	$T_{s\&g}$
1	74	91	144	123
2	84	124	214	198
3	144	345	681	681

Fig. 15 shows the strong impact of the combined actions of OEL and OLTC on the nose shape, for Case 1 and Condition 2. Three seconds before T_{max} the OEL begins to operate in closed loop with a dominant time constant of few seconds.

Again Case 3 is not able to correctly reconstruct in the values and in the time, the real process that moves according to the Cases 1 and 2 dynamics.

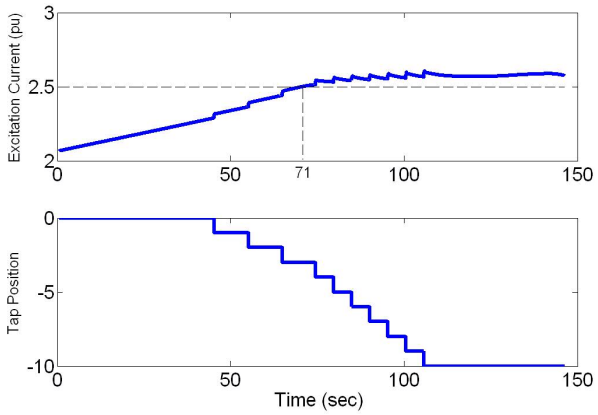

Fig. 15. Excitation Current and Tap Position in Case 1 Simulation

C. *P-constant Load Type ($\alpha = \beta = 0.0$)*

All results in this subsection were obtained with the load represented as P-constant type. Fig.16 and Fig.17 show the nose curves when the system is in Condition 1 for Bus#3 and Bus#5, respectively. Fig.18 and Fig.19 show the nose curves when the system is in Condition 2 for Bus#3 and Bus#5, respectively.

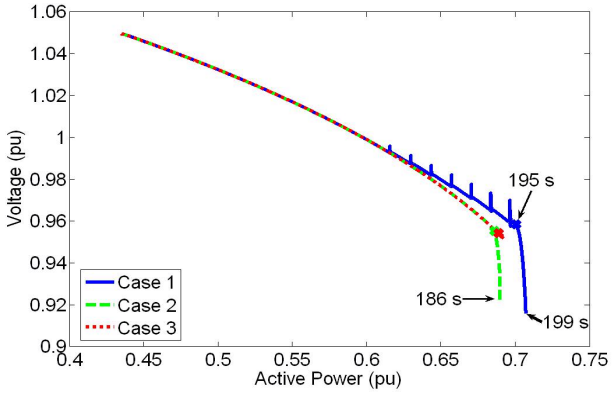

Fig. 16. Nose Curves at Bus#3 for Condition 1 and load as P-constant

Table V shows the times with respect to the simulation results presented in Fig.16.

Table V– Key recorded time (sec) with respect to Fig.16

Case	T_{max}	$T_{0.85}$	T_{coll}	$T_{s\&g}$
1	199	> 199	199	195
2	186	> 186	186	184
3	189	> 189	189	186

Comments on Fig.16 and Table V

13. In all three cases the voltage instability is mainly driven by the OEL dynamics;
14. The instability occurs before the maximum power transfer point. Only points at the upper part of the nose curve can be shown.
15. The instability occurs at a high voltage profile. This confirms that relying voltage instability proximity indication on voltage profile only, is not a safe procedure.
16. With this load type Case 3 is able to represent with good approximation the real process performance.

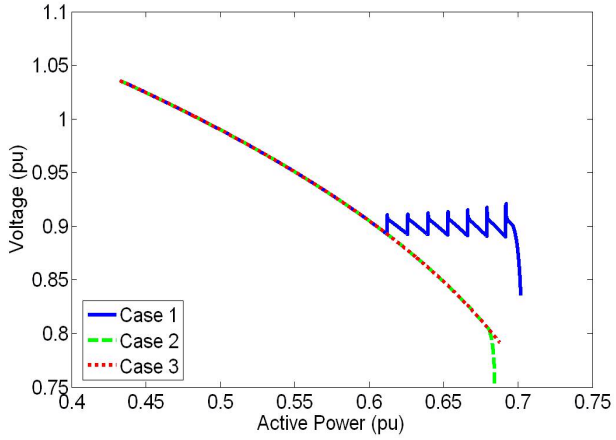

Fig. 17. Nose Curves at Bus#5 for Condition 1 and load as P-constant

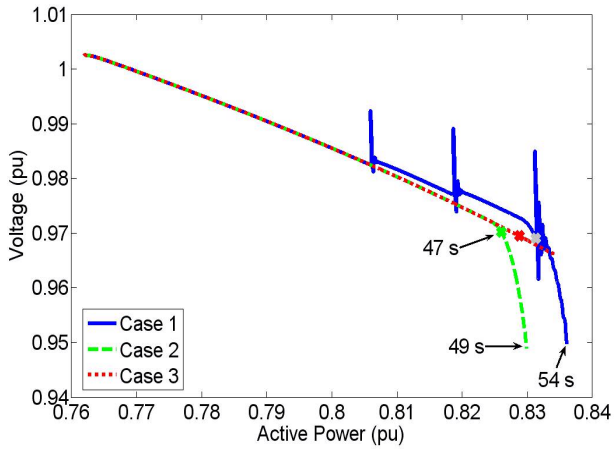

Fig. 18. Nose Curves at Bus#3 for Condition 2 and load as P-constant

At Bus#5 the voltage lowering is more evident, as in all the performed tests.

Table VI shows the times with respect to the simulation results presented in Fig.18, and Fig.20 shows again the combined actions of OEL and OLTC determining the beginning of voltage instability for Case 1 and Condition 2.

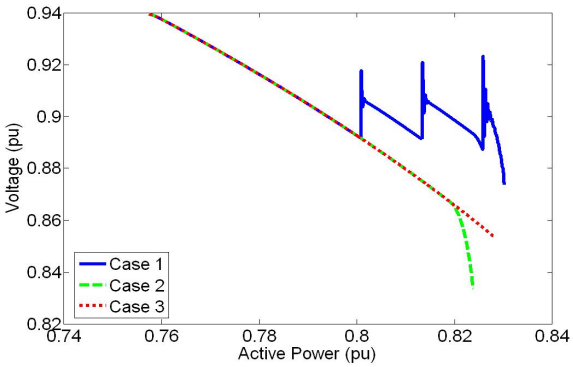

Fig. 19. Nose Curves at Bus#5 for Condition 2 and load as P-constant

Table VI– Key recorded time (sec) with respect to Fig.18

Case	T_{max}	$T_{0.85}$	T_{coll}	$T_{s\&g}$
1	54	> 54	54	51
2	49	> 49	49	47
3	53	> 53	53	49

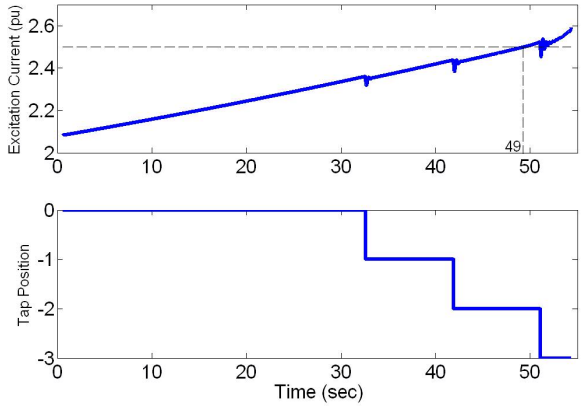

Fig. 20. Excitation Current and Tap Position in Case 1 Simulation

The main results of the comprehensive analysis made in this section are the following:

- The static PV curve is very different from the possible dynamic ones with the exception of the P-constant load case;
- The real voltage instability is always determined by OEL or by the combined action of the OEL and OLTC.

Now the analysis necessarily moves from an organic but theoretical approach to a more realistic system contest, where the load seen by the EHV bus is generally represented by a combination of the previously considered theoretical typologies.

V. PV Curve Analysis for a More Realistic Generic Load Representation

In this section the simulations are performed considering the load characteristic having $\alpha = 0.7$ and $\beta = 2.0$. These

coefficients are the ones used in the simulations for the Italian system to be presented in the next section.

Fig.21 and Fig.23 show the nose curves of Bus#3 and Bus#5, respectively. The real load analysis confirms the relevant differences between the nose of the static PV curve (Case 3) and the dynamic ones (Cases 1 and 2) for both the EHV (Bus#3) and the LV (Bus#5) buses. More precisely:

- The maximum loadability differs of about 7%;
- The instability begins at very high voltages and at a time very different between Case 3 and Cases 1 and 2, as also shown in Table VII, with differences of about 300s;
- It is clearly confirmed, as also shown in Fig. 22, the relevant effect of the OEL alone or in combined action with the OLTC, in the triggering of the real voltage instability.

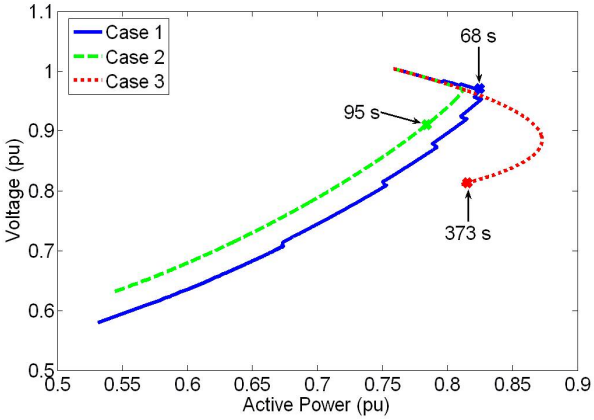

Fig. 21. Nose Curves at Bus#3 for Condition 2 with the load represented as a generic dynamic model

Table VII shows the times with respect to the simulation results presented in Fig.21.

Table VII– Key recorded time (sec) with respect to Fig.21

Case	T_{max}	$T_{0.85}$	T_{coll}	$T_{s\&g}$
1	74	86	97	68
2	79	104	118	95
3	260	322	374	373

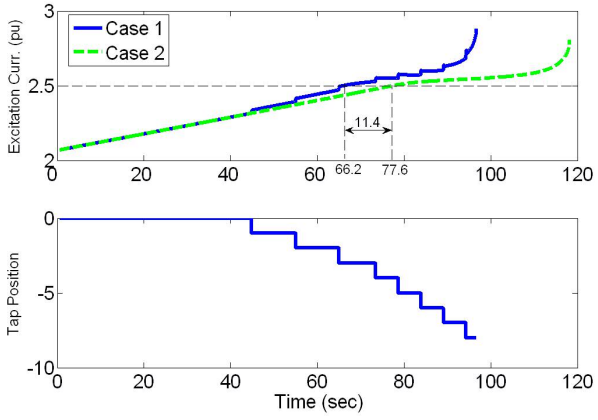

Fig. 22. Excitation Currents in Cases 1 and 2 and Tap Position in Case 1

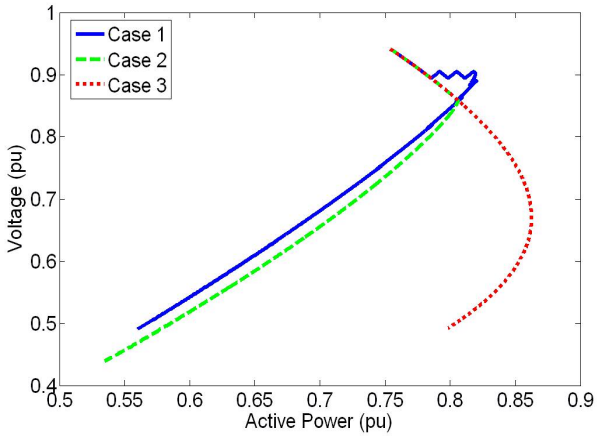

Fig. 23. Nose Curves at Bus#5 for Condition 2 with the load represented as a generic dynamic model

To give a better understanding of $T_{s\&g}$, Fig.24 shows the voltage at Bus#3 for the cases where the load increase stops at 67 sec (dashed line) and at 68 sec (solid line). At 40 sec the voltage at Bus#5 reaches 0.9 pu triggering the OLTC clock. At 45 sec the first tap position is changed in order to support the voltage at Bus#5. The subsequent tap changes occur at 55, 65, 74, 82, 88, 93, 98, 103, 108 sec. At 66 sec the OEL starts to actuate. So, the evolution of the OEL and OLTC dynamics combined with the time the load increase stops, drives the stability of the system.

In other words, when the load increase stops at 67 sec the stability boundary is not crossed and the system dynamics find a stable equilibrium. On the contrary, when the load increase stops at 68 sec the stability boundary is crossed and the dynamics of the system do not find a stable equilibrium.

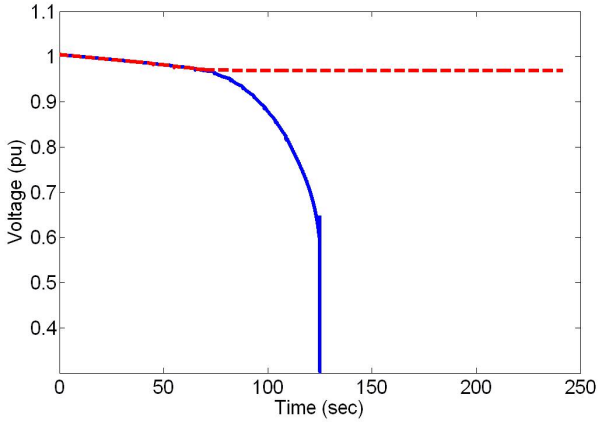

Fig. 24. Voltages at Bus#3 when stopping the load increase at 67s (dashed) and at 68s (solid)

All the above results give a clear evidence and confirm the statements a), b), c), and d) anticipated in the Introduction Section. Lastly, the 30s difference between T_{coll} and $T_{s\&g}$, in Case 1, clearly shows the different meaning between voltage instability and the loss of convergence in the system computing.

VI. PV Curve Analysis for the Italian System

This section has the objective to compare the performances of the proposed equivalent dynamic model with the results of a wide, detailed, multivariable, dynamic model of a large power system.

The Italian system analyzed contains the 380kV and 220kV networks (Fig.25 depicts the 380kV network only). The system configuration has 2549 buses, 2258 transmission lines, 134 groups of thermal generators and 191 groups of hydro generators. The system load is approximately 50 GW, fully represented as a static model (2) with α=0.7 and β=2.0. Similarities on test results have shown that representing the loads with 50% static model and 50% dynamic model with a power restoring time constant of 5 sec, were not worth showing. The system is under primary voltage and frequency control only.

Two set of tests were performed, one at the Milano Area (Region A marked in Fig.25 and enlarged in Fig.26), and another at the Firenze Area (Region B marked in Fig.25 and enlarged in Fig.27). The analysis performed in Milano Area consisted of increasing the local area by a rate of 10%/min maintaining constant the power factor. In order to enforce a voltage instability to a given bus, which gave us the opportunity to monitor the critical bus, we increased the load at Brugherio 380kV bus at a rate of 20%/min. The load at Brugherio is fed through three 380kV/132kV OLTC transformers.

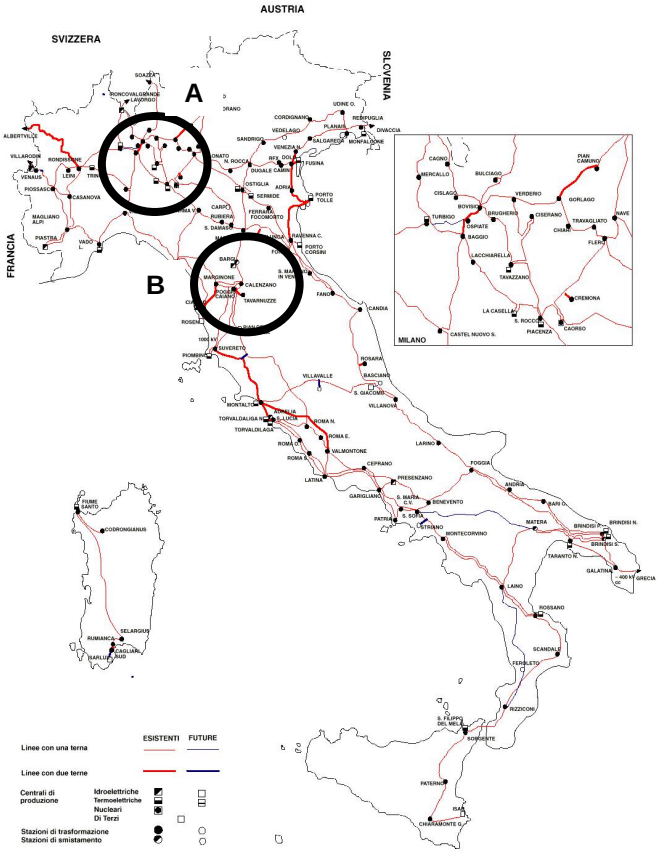

Fig. 25. 380kV Italian Network

Fig. 26. Enlarged detail of the area "A" marked in Fig. 25

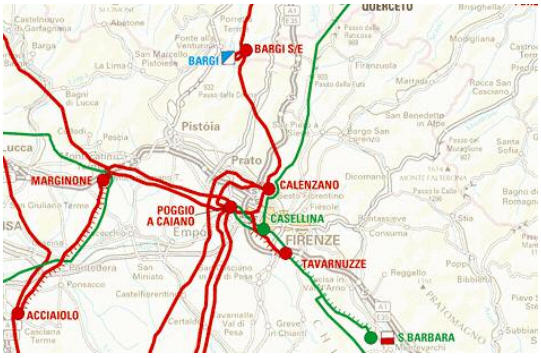

Fig. 27. Enlarged detail of the area "B" marked in Fig. 25

Fig.28 shows the nose curves of the Brugherio 380kV bus in four cases described as follows:

- Case 1 – all OELs in service and only Brugherio OLTCs in service;
- Case 2 – all OELs in service and all OLTCs out of service;
- Case 3 – all OELs and OLTCs out of service;
- Case 4 – all OELs and OLTCs in service.

Case 1 better fits the equivalent dynamic model with OLTC given in Fig.5. Case 4 represents a more realistic situation to which Case 1 has to be compared. Case 2 is another realistic condition with all OLTCs blocked. Case 3, as before, represents the reference due to its close approximation to the static PV curve.

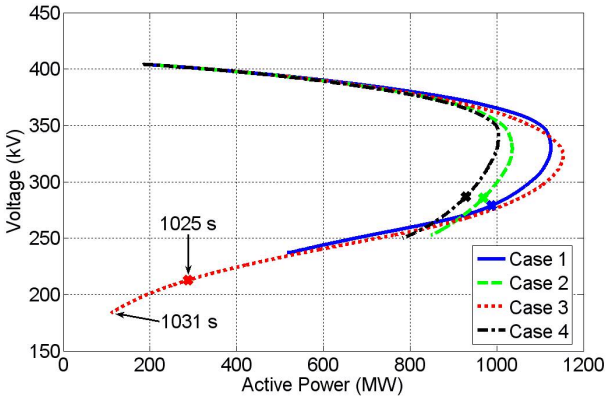

Fig. 28. Nose Curves for Brugherio 380kV Bus

Fig.29 shows the tap positions of the three Brugherio OLTC transformers for Case 1. It can be seen that a continuous tap variation model was employed in the SICRE simulator [15]. The OLTCs cease to operate when their tap position reaches the non dimensional value of 0.8 (lower tap limit). Fig. 30 shows the tap position, in Case 4, of the three OLTC transformers in Brugherio (the three heavier solid lines) and the other OLTCs working in the same grid area (lighter solid lines). It can be seen that the Brugherio OLTCs reach their lower tap limits before the others, due to the load increase profile, which enforced a higher increase rate at the Brugherio bus.

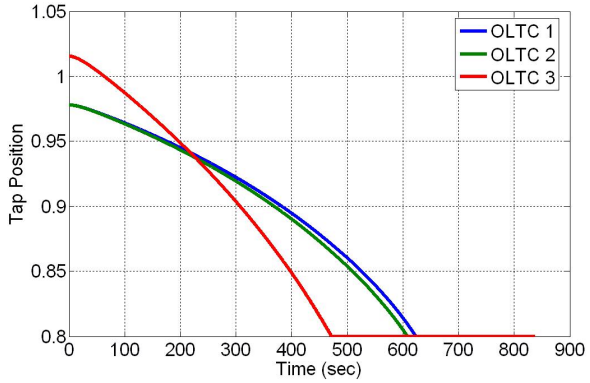

Fig. 29. Brugherio tap evolution corresponding to Case 1

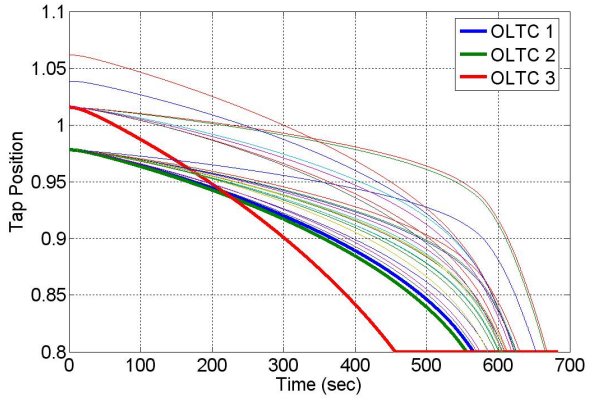

Fig. 30. Brugherio tap evolution corresponding to Case 4

Table VIII shows the times with respect to the simulation results presented in Fig.28 for the Brugherio 380kV bus. $T_{0.85}$ was defined for a base voltage of 400kV, i.e., it is the time when the voltage reaches 340kV.

Table VIII – Key recorded time (sec) with respect to Fig.28

Case	T_{max}	$T_{0.85}$	T_{coll}	$T_{s\&g}$
1	715	686	838	805
2	740	710	845	815
3	881	800	1031	1025
4	585	587	684	660

Fig.31 shows OEL indicators for Case 1 of some of the large groups of generation electrically close to the Brugherio 380kV bus. The closest groups are Tavazzano1, Tavazzano2 and Turbino showed in heavy solid lines. When this indicator reaches zero, the machine over-excitation limiter begins to work in closed loop. Three other groups (Vado, Spezia and La Casella) although electrically farther to Brugherio reach their over-excitation limits before Tavazzano and Turbigo due to their higher initial excitation condition. Fig.32 shows the OEL indicators for Case 4. One can note that when all the OLTCs are unblocked (Case 4), Tavazzano's and Turbigo's OEL start to operated 100s before with respect to their operation in Case 1, where only Brugherio's OLTCs are unblocked.

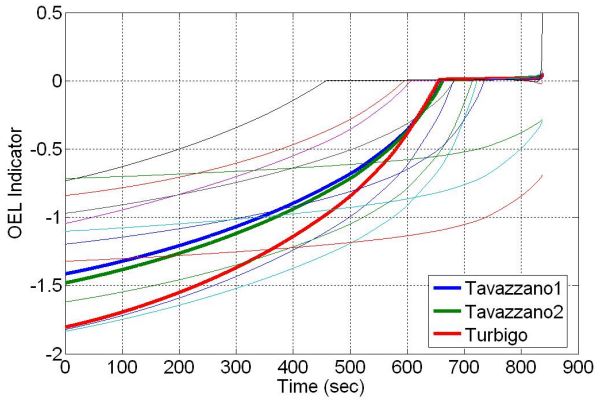

Fig. 31. OEL Indicators corresponding to Case 1

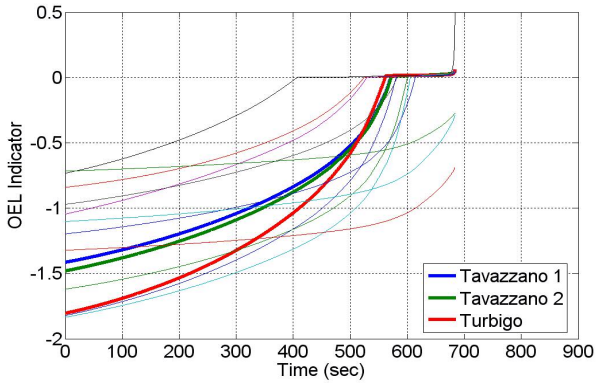

Fig. 32. OEL Indicators corresponding to Case 4

The comparison of the results presented in Section V with the ones presented in Section VI is of real interest mainly concerned with the general trends of the nose curves and with the voltage instability point along them. Due to the natural difficulties to compare the operating conditions of the two systems, the analyses present relevant numerical differences, which will be later clarified. Starting from Cases 3, both show instability at low voltage values, particularly in the Italian system, and with relevant delay with respect to the other more realistic cases. For Cases 1, both nose tips are reached at higher voltage values than the corresponding Case 3 tips. The main difference is between the two points corresponding to $T_{s\&g}$ – the one in Fig.21 is located on the nose tip while the other on Fig.28 at a low voltage below the nose tip.

The continuous integrator law utilized in the Italian system OLTCs do not give rise to the saw-teethed shape as seen in Fig.21, where a discrete stepping control law is used in the OLTC of the equivalent model. Comparing Cases 2, the nose

shape is smoother in Fig.28 due to the different time the large amount of the generators in the Milano Area (instead of the single generator in Fig.21) reach their OEL re-closure. This is also the reason why the time span between the OEL operation in Tavazzano and Turbigo (Fig.32 – Case 4) and the $T_{s\&g}$ value (660s in Table VIII) is not small (approximately 100s).

For Cases 1, the large system shows the instability point at low voltage, whereas the small system shows this point at high voltage. The main reason for this difference is due to the local OLTCs that, in the large system, have already reached their saturation before the local OELs begin to operate. Therefore, the lack of simultaneous operation of OELs and OLTCs is the main reason of the noticed delay and lower voltages in Fig. 28.

Case 4 is the most realistic of the four cases, only comparable with the other curves in Fig.28. It clearly shows that the combined actions of OELs and OLTCs makes the nose shorter with respect to Case 2, and anticipates the time of instability. From the comparison with Case 3, representing the static PV curve, the difference in terms of loadability and voltage instability timing are very large.

The load difference at the tip, between Case 3 and Case 2 is of about 10% in Fig.28 and 7% in Fig.21. Moreover, Table VIII shows large difference in time between Case 3 and the other cases, again confirming the inadequacy of the PV static curve to correctly describe the voltage lowering and the voltage instability.

Fig.33 shows the nose curves of the Poggio a Caiano 380kV bus in four cases described as follows:

- Case 1 – all OELs in service and only the Poggio a Caiano OLTC in service;
- Case 2 – all OELs in service and all OLTCs out of service;
- Case 3 – all OELs and OLTCs out of service;
- Case 4 – all OELs and OLTCs in service.

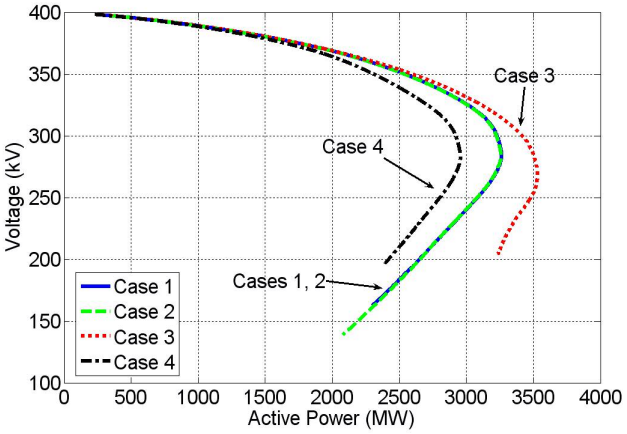

Fig. 33. Nose Curves for Poggio a Caiano 380kV Bus

The proximity of the curves for Cases 1 and 2 differs from the Fig.28 results. It is explained by the fact that at Poggio a Caiano 380kV bus there is a large part of the local load fed directly at 380kV. Only a small part of the local load (25%) is fed through OLTC transformers at the Casellina 220kV bus (see Fig.27). According to that, the Case 1 nose in Fig.28 is closer to Case 3 nose, whereas in Fig.33 it is closer to Case 2 nose.

Table IX – Key recorded time (sec) with respect to Fig.33

Case	T_{max}	$T_{0.85}$	T_{coll}
1	1279	933	1329
2	1287	937	1338
3	1458	966	1602
4	1160	838	1206

Again, Fig. 33 and Table IX confirm the relevant differences in the maximum loadability and in the time to collapse between the static and dynamic PV curves.

In conclusion, evidence is given to the ability of the proposed equivalent dynamic model to represent the real system process of voltage degradation and voltage collapse, even if Case 4 gives room to a possible improvement (see next Section).

It is worth noting that in the tests made in the Italian network the maximum load is generally reached at a voltage profile lower than 0.85 pu. Thus, before reaching the maximum loadability point, protective relaying not represented in the simulations will actuate. If the secondary voltage control [16,17] were present, the nose curves shown in Fig.28 and Fig.33 would have a flatter shape at the upper part. A comprehensive analysis of the impact of the secondary voltage control in the nose curves is out of the scope of this paper.

VII. Opening Discussions

The proposed dynamic model is, in the authors' opinion, a satisfactory equivalent representation of the real system, at a given bus. The most important dynamic aspects linked to the voltage instability are taken into account, including the OLTC at the considered bus. The OLTC representation at the remaining system should require a more complex equivalent model in terms of structure and control parameters, not easy to be defined. The other not-too-far OLTCs impact the nose curve of the considered bus by lowering the maximum loadability, and by anticipating the instability point. These effects can be better reproduced through the equivalent dynamic model by adding, in Fig.5, a new bus electrically close to the considered one, along the transmission lines, having a local equivalent OLTC and load. Obviously, the parameter values of this more complex model could change according to the considered bus and therefore based on the characteristics of the surrounding network.

The relevant differences in terms of loadability and time for instability among a static and dynamic model allow to say that only the dynamic model is able to show the correct nose shape and instability point. In fact, starting from a common equilibrium point for both static and dynamic models, the process degradation due to the load increase up to the maximum power transfer into the considered bus, will show two different PV curves. These curves present large differences on the time to run along them, and therefore, on

the amount of load increase required to reach their different maximum loadability values.

The paper confirms that the tips of the nose curves do not correspond to the voltage instability point, even in the case of a P-constant load when the system dynamics are considered. In the case of a P-constant load the instability occurs a short time before the tip. In the other cases, the instability normally occurs after the tip of the nose, going farther along the curve as higher is the Z-constant portion. According to that, any voltage instability indicator based on the maximum loadability finding, would appear not precise, mainly in the presence of a real load.

The operation of the OELs is very relevant in triggering the voltage instability under certain operating conditions. Nevertheless, the time span between the local OELs operation and the voltage instability could be large. Therefore, the real-time information about the OELs operation should cover a large part of the grid around the considered bus. The availability (still very difficult in practice for real time use) of this large amount of data, put anyhow, the problem to correctly decide when it is the time to consider them very critical for the voltage instability.

The paper shows the high speed on the voltage lowering after the tip nose, before the real instability. In practice this still stable but fast changing operating condition appears of interest, more than the first, instable point, at very low voltage. Therefore the beginning of fast voltage lowering should be the point to be recognized to increase the system security and reliability. According to that, the maximum loadability point really represents the "gate" after which the fast voltage lowering becomes very critical, with risk of protection interventions and system security degradation.

In the performed analysis, it is worth noting that a dynamic representation of the load (determining a partial power self-restoration with a time constant of about 5s), did not qualitatively changed the major results of the paper. Since all the simulations are based on a gradual and continuous increase of the load admittance, in our experience, the slow power recovery being taken into account, plays a secondary role on the values and stability of the PV curve equilibrium points, where the primary role is played by the voltage control and excitation limiters.

About the load characteristic impact on the loadability and voltage instability point, one is driven to think about the usefulness of the PV curve analysis on voltage instability when considering loads as P-constant, I-constant, and Z-constant (see the analysis in Section IV). Is it simply an academic exercise to understand better the mixed ZIP load cases or they have a real meaning? For example, the case of P-constant is very far from the correct result, that notwithstanding it is largely used! In the authors' opinion, it becomes realistic only when the Thevenin equivalent is redefined at each step by transferring the Z-constant and I-constant portions of the actual load inside the equivalent Thevenin impedance [12]. In doing that, the new PV curve maximum loadability point should correspond, in terms of time and voltage value, to the correct voltage instability point determined by the load-independent Thevenin equivalent.

For voltage instability proximity indication based on local phasor measurements, the identification of the two parameters of the simple equivalent circuit given in Fig. 1 should require, according to the paper results, a very fast computation. In fact, especially during the fast voltage degradation period, determined by the combined actions of the OELs and OLTCs, the PV curve equilibrium points quickly change value and must be adequately tracked. This implies that the off-line parameter identification methods related to a specific, normal operating condition or the ones on-line but slow in the identifying and updating parameters are not appropriate for the precise and on-time voltage instability risk indication.

Even though we understand that in "highly specialized load flow programs" the static model can detect the voltage instability, considering that the "statics" correspond to the underlined dynamic model [18], we think that to be able to perfectly achieve this correspondence is not a trivial task. One example that supports our concerns is the correct modeling of the OLTC dynamics, which should be modeled as a set of algebraic equations governed by time delays, voltage thresholds, and furthermore, the restriction to change the tap only between subsequent positions. Another example is the OEL effect that is not precisely described by changing a generator bus from a PV to a PQ type. The OEL modifies the reactive power during its operation under load increase, and being an active closed-loop control, it has an impact on the stability characteristics of the PV curve equilibrium points.

VIII. Conclusions

This paper analyzed the voltage stability problem by showing the strong impact of OELs and OLTC transformers on the shape of the PV curve and on the speed the equilibrium point runs along the curve. The results show that the Thevenin equivalent of the grid seen by a given EHV bus cannot be simply represented by a constant-voltage generator feeding the load by a constant reactance. The relevant differences between the static and the dynamic equivalent models are put in evidence in terms of maximum loadability, running speed along the PV curve and instability of part of the equilibrium points. A large detailed grid confirms the results of the proposed dynamic equivalent model.

Voltage instability indicators based on local phasor measurements at a given EHV bus, should therefore be in link with the issues focused in this paper. They have to be able to identify the parameters of the equivalent system in Fig.1, when the generator voltage and line reactance values quickly change as the instability point approaches (i.e., when OELs and OLTCs are working). Thus, the correct and fast estimation of the Thevenin parameters dependent on the control system dynamics is of paramount importance. More precisely:

- The relevant difference of the dynamic model is in the lower loadability, in the faster voltage lowering around the tip of the nose, and in the instability of its low voltage equilibrium points, dependent on load characteristics;

- The tip of the nose does not necessarily represent the voltage instability limit. Often, the real instability is at lower voltage value;
- Fast, voltage reductions even in front of slight load increase, do not always correspond to a voltage instability but rather to a fast lowering preceding the real instability;

From the practical viewpoint of real systems other considerations have to be pointed out:

- Under the voltage threshold of 85%, possible emergency control systems, SPS and protections begin to work due to either a correct or an untimely operation;
- Either the static or the dynamic PV curves always reach the maximum loadability at voltage values not higher than the threshold of 85%. Therefore the real voltage instability limit, at very low voltage, is of more theoretical than practical interest;
- In practice, only the upper curvature of the nose before the tip, where the PV curve points are all stable but quickly lowering, in front of small load increase, is of interest.
- The growing speed of the voltage lowering when approaching the nose tip is the main reason of real interest to identify/predict the maximum loadability point;
- The identification of the static Thevenin equivalent, when approaching the nose tip, should be very fast with high slope change on E_{Th} and X_{Th} values to approximate as better as possible the performance of the corresponding dynamic equivalent model, which is the only one able to correctly reconstruct the real phenomena (OEL and OLTC effects);

To conclude, the static model of the Thevenin equivalent, with fixed E_{Th} and X_{Th} values gives a sluggish and wrong indication of the voltage instability/maximum loadability. On the contrary, the equivalent dynamic model is able to correctly describe the real power system seen by a given EHV bus and therefore the correct shape of the PV nose curve. This means that only a fast identification method of variable E_{Th} and X_{Th} parameters allows to correctly and timely recognize the maximum loadability point.

IX. Acknowledgements

The authors would like to acknowledge Ferdinando Parma, Massimo Salvetti and Massimo Pozzi for their contributions regarding the SICRE simulator, and Giuseppe Cappai and Ivan Valade for their contributions regarding the DigSilent simulator.

X. References

1. C. W. Taylor, *Power System Voltage Stability*, New York, McGraw-Hill, 1994.
2. P. Kundur, *Power System Stability and Control*, New York, McGraw-Hill, 1994.
3. T. Van Cutsem and C. Vournas, *Voltage Stability of Electric Power Systems*, Norwell, MA, Kluwer, 1998.
4. V. Ajjarapu and B. Lee, "Bibliography on voltage stability," *IEEE Transaction on Power Systems*, Vol. 13, No. 1, pp. 115-125, 1998.
5. J. Deuse and M. Stubbe, "Dynamic simulation of voltage collapses," *IEEE Transactions on Power Systems*, Vol. 8, No. 3, pp. 894-904, August 1993.
6. G. K. Morison, B. Gao and P. Kundur, "Voltage stability analysis using static and dynamic approaches," *IEEE Transactions on Power Systems*, Vol. 8, No. 3, pp. 1159-1171, August 1993.
7. R. J. Koessler and J. W. Feltes, "Time-domain simulation investigates voltage collapse," *IEEE Computer Applications in Power*, Vol. 5, pp. 18-22, October 1993.
8. B. Gao, G. K. Morison and P. Kundur, "Towards the development of a systematic approach for voltage stability assessment of large-scale power systems," *IEEE Transactions on Power Systems*, Vol. 11, No. 3, pp. 1314-1324, August 1996.
9. T. Van Cutsem, "Voltage Instability: Phenomena, Countermeasures, and Analysis Methods, *Proceedings of the IEEE*, Vol. 88, No. 2, pp. 208-227, February 2000.
10. A. G. Phadke, "Synchronized Phasor Measurements in Power Systems", *IEEE Computer Applications in Power*, Vol. 6, No. 2, pp. 10-15, April 1993.
11. K. Vu, M. M. Begovic, D. Novosel and M. M. Saha, "Use of Local Measurements to Estimate Voltage-Stability Margin", *IEEE Transactions on Power Systems*, Vol. 14, No. 3, pp. 1029-1035, August 1999.
12. B. Milosevic and M. Begovic, "Voltage-Stability Protection and Control Using a Wide-Area Network of Phasor Measurements", *IEEE Transactions on Power Systems*, Vol. 18, No. 1, pp. 121-127, February 2003.
13. G. Verbic and F. Gubina, "A New Concept of Voltage-Collapse Protection Based on Local Phasors", *IEEE Transactions on Power Delivery*, Vol. 19, No. 2, pp. 576-581, April 2004.
14. I. Smon, G. Verbic and F. Gubina, "Local Voltage-Stability Index Using Tellegen's Theorem", *IEEE Transactions on Power Systems*, Vol. 21, No. 3, pp. 1267-1275, August 2006.
15. E.Cima, B. Cova, R. Marconato, G. Salvadori, R. Salvati, P. Scarpellini: "A Powerful Simulator for Investigating Severe Dynamic Phenomena During System Major Distarbance", Paper No. 38-305, *CIGRE Session*, Paris, August 1996.
16. S. Corsi, M. Pozzi, C. Sabelli and A. Serrani, "The Coordinated Automatic Voltage Control of the Italian Transmission Grid – Part I: Reasons of the Choice and Overview of the Consolidated Hierarchical System," *IEEE Transactions on Power Systems*, Vol. 19, No. 4, pp. 1723-1732, November 2004.
17. S. Corsi, M. Pozzi, M. Sforna and G. Dell'Olio, "The Coordinated Automatic Voltage Control of the Italian Transmission Grid – Part II: Control Apparatuses and Field Performance of the Consolidated Hierarchical System," *IEEE Transactions on Power Systems*, Vol. 19, No. 4, pp. 1733-1741, November 2004.
18. I. Dobson, Discussion on Bifurcation Theory and Modal Analysis posted in *Power-Globe List*, May 2006.
19. IEEE Task Force on Excitation Limiters, "Recommended models for overexcitation limiting devices", *IEEE Transactions on Energy Conversion*, Vol. 10, No. 4, pp. 706-713, Decembert 1995.

XI. Appendix

Fig.34 shows the block diagram of the automatic voltage regulator (AVR) and the over-excitation limiter (OEL).

The OEL model is of the summing type with soft limiting, which retains the normal voltage regulator loop [19].

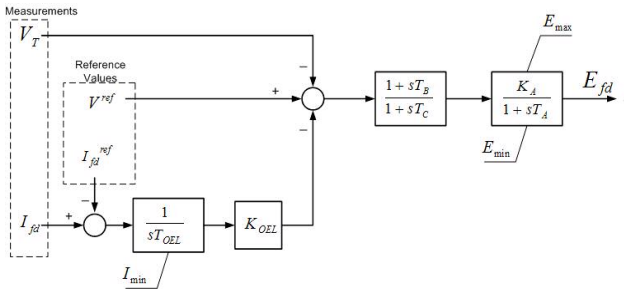

Fig. 34. AVR and OEL block diagram

AVR and OEL

K_A =500 pu/pu, T_A =0.03 s, T_B =1.0 s, T_C =10 s, K_{OEL} =1.0 pu/pu, T_{OEL} =10 s, I_{fd}^{ref} =2.5 pu, V^{ref} =1.03 pu, $E_{\max}$ =5 pu, $E_{\min}$ =-1 pu, $I_{\min}$ =0.0 pu.

Fig.35 shows the block diagram of the speed regulator.

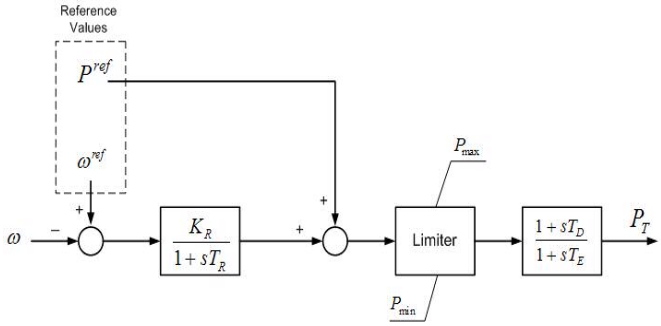

Fig. 35. Speed regulator block diagram

Speed Regulator

K_R =20 pu/pu, T_R =0.04 s, T_D =3.0 s, T_E =10 s, $P_{\max}$ =0.9 pu, $P_{\min}$ =0.0 pu, P^{ref} is either 160/370 pu or 280/370 pu depending on the operating condition under analysis.

Generator

H =9.26 s, D =0.0 pu/pu, r_a =0.0014 pu, x_l =0.193 pu, x_d =1.9 pu, x_q =1.7 pu, T_d' =1.27 s, T_q' =0.235 s, x_d' =0.302 pu, x_q' =0.5 pu, T_d'' =0.027 s, T_q'' =0.012 s, x_d'' =0.204 pu, x_q'' =0.3 pu.

Overhead Transmission line

Length=100km, rated voltage = 400kV, rated current = 1kA, nominal frequency = 50Hz, resistance = 0.029Ω/km, reactance = 0.3833Ω/km, susceptance = 2.859μS/km

Step-up transformer

Rated power=380MVA, HV-side = 400kV, LV-side=20kV, r=0.1896%, xl=12.68%, xm=0.18%, rf=0.0

Step-down transformer

Rated power=460MVA, HV-side = 400kV, LV-side = 132kV, r=0.1638%, xl=14.66%, xm=0.26%, rf=0.0

Distribution OLTC transformer

Rated power = 64MVA, HV-side = 132kV, LV-side = 20kV, r=0.4406%, xl=22.5%, xm=0.5%, rf=0.078%, additional voltage per tap = 1.25%.

OLTC mechanism

Senses LV-side, minimum tap changer delay = 5s (initial and subsequent), Min Voltage = 0.9pu, Max voltage = 1.1pu, min tap position = -10, max tap position = 10.

XII. Biographies

Sandro Corsi (M'89, SM'06) received the Doctorate degree in electronics (automatic systems) from the Polytechnic of Milan, Milan, Italy, in 1973. In 1975, he joined ENEL's Automatic Research Center, where his main interests were power system voltage control, generator control, power electronics devices, advanced control technology, and power system automation. He was a Research Manager at ENEL S.p.A. Ricerca beginning in 1997, in charge of the Power System Control and Regulation Office. After ENEL reorganization, he was a Research Manager at CESI, Milan, in charge of the Network and Plant Automation Office from 1999 and of the Electronics and Communications Office in the Automation Business Unit from 2000. Since 2001, he has been with CESI R&D and Sales. He is author of more than 60 papers on system control. Dr. Corsi is a Member of CIGRE, IEEE-PES, CEI, and the IREP Board.

Glauco N. Taranto (S'92, M'96, SM'04) was born in Rio de Janeiro, Brazil, in 1965. He received the B.Sc. degree in 1988 from the State University of Rio de Janeiro, Rio de Janeiro, the M.Sc. degree in 1991 from the Catholic University of Rio de Janeiro, and the Ph.D. degree in 1994 from Rensselaer Polytechnic Institute, Troy, NY, all in Electrical Engineering. In 2006, he was on sabbatical leave as a Visiting Fellow at CESI, Milan, Italy. Since 1995, he has been with the Electrical Engineering Department at the Federal University of Rio de Janeiro/COPPE, Brazil, where he is currently an Associate Professor. His research interests include power system dynamics and controls, intelligent control, and robust control design. Dr. Taranto is a member of the IEEE PES and CSS, Power System Dynamic Performance Committee and CIGRE.